OPEN ACCESS
JOURNAL OF ADVANCED DIELECTRICS
Vol. 12, No. 3, (2022) 2250002 (6 pages)

DOI: 10.1142/S2010135X22500023

Piezoelectric, ferroelectric and pyroelectric properties of $(100–x)Pb(Mg_{1/3}Nb_{2/3})O_3–xPbTiO_3$ ceramics

Chuan Chen*,†, Yan Wang*,†, Jiajiu Li‡,¶, Chaofeng Wu§ and Guanrong Yang‡

*Electric Power Intelligent Sensing Technology and Application State Grid Corporation Joint Laboratory
Future Science Park, Changping District, 102209 Beijing, P. R. China

†Department of Electric Power Sensing Technology, Global Energy Interconnection Research Institute co., Ltd.
Future Science Park, Changping District, 102209 Beijing, P. R. China

‡Foshan (Southern China) Institute for New Materials, Nanhai District, 528200 Foshan, P. R. China

§Center of Advanced Ceramic Materials and Devices, Yangtze Delta Region Institute of Tsinghua University
314006 Zhejiang, P. R. China

¶1026254157@qq.com

Received 3 November 2021; Revised 6 January 2022; Accepted 4 February 2022; Published 4 March 2022

A series of $(100–x)Pb(Mg_{1/3}Nb_{2/3})O_3–xPbTiO_3$ (PMN–*x*PT, x = 24, 25, 26) ceramics were prepared by solid-state reaction technique using $MgNb_2O_6$ precursor. The results of the detailed characterizations reveal that the content of PT has negligible influence on the grain size, and all samples possess the perovskite structure. As the PT content increases, the samples changed from the normal ferroelectric phase to the ergodic relaxor state at room temperature. As a result, PMN–*x*PT ceramics are endowed with electro-strain of 0.08% at a relatively low electric field of 2 kV/mm, and effective piezoelectric coefficient of 320 pm/V was obtained. Simultaneously, the PMN–*x*PT ceramics have exceptional pyroelectric performance, exhibiting a high pyroelectric coefficient p~5.5 – 6.3 × 10^{-8} C·cm^{-2}·K^{-1}. This study demonstrates the great potential of PMN–*x*PT for piezoelectric and pyroelectric device applications.

Keywords: Perovskite; PMN–PT; electro-strain; ferroelectric phase.

1. Introduction

Lead-based relaxor ferroelectric materials are generally binary or ternary solid solutions of $PbTiO_3$, represented by $PbZrO_3$–$PbTiO_3$ (PZT), $Pb(In_{1/2}Nb_{1/2})O_3$–$Pb(Mg_{1/3}Nb_{2/3})$–$PbTiO_3$ (PIN–PMN–PT) and $Pb(Mg_{1/3}Nb_{2/3})O_3$–$PbTiO_3$ (PMN–PT).[1–3] They have typical ABO_3 perovskite structure, and the general formula of their composite perovskite structure is A $(B'B'')O_3$ or $A'A''(B'B'')O_3$, which is characterized by more than one ion at the same lattice position. Their excellent ferroelectricity, high dielectric properties, strong piezoelectric performance and good pyroelectric, photoelectric properties render them widely used in ferroelectric memory, actuators, sensors, dielectric resonators and transducers.[4–7] $(100–x)Pb(Mg_{1/3}Nb_{2/3})O_3–xPbTiO_3$, (where x varies from 0 to 100), where the A-site ion is Pb^{2+}, the B-site ions are composite ions (B′ is Mg^{2+} and B″ is Nb^{5+}).[8,9] It displays a broader dielectric dispersion around Curie temperature (T_C), a higher dielectric constant, and a relatively small dielectric temperature coefficient. Therefore, this material can be widely used in consumer electronic products, pulse power applications and energy harvesting systems.[10–12]

For the binary solid solution systems with different PT contents in PMN–PT, due to different phase structure, the corresponding structures and properties are also different. On both sides of the MPB phase boundary component, one side with low PT content shows strong dielectric relaxation characteristics, while the other side shows typical ferroelectric characteristics.[13–15] However, PMN–PT binary system also undergoes different types of phase transition, which depends on the value of x, and its crystal structure will change significantly with temperature. At low temperature (below Curie temperature), when the PT content is less than 27, PMN–PT system shows a rhombohedral structure (R), and when the PT concentration was higher ($x > 34$), it showed a tetragonal structure (T). Therefore, in the MPB component region ($27 < x > 34$), PMN–PT system is the coexistence of rhombohedral and tetragonal phases. Above the Curie temperature, no matter what the PT content is, the crystal structure of the PMN–PT system is a cubic phase without the piezoelectric effect.[16–18]

It is well known that PMN–PT has excellent piezoelectric properties in rhombohedral phase region, tetragonal phase region and MPB region. Especially, PMN–PT ceramics near MPB have very high piezoelectric coefficient, extremely high electro-strain and excellent electromechanical coupling factors, which are far greater than those of PZT-based

¶Corresponding author.

ceramics. PMN–PT ceramics can be used to fabricate high sensitivity ultrasonic transducers, large displacement actuators and sensors. PMN–PT ceramics have good application prospects in ultrasonic imaging and sonar positioning systems.[19–21] Therefore, in this work, (100–x)PMN–xPT (x = 24, 25, 26, these component are close to MPB) was selected and prepared by solid-state reaction. $MgNb_2O_6$ precursor route was used for synthesis to reduce the possible formation of pyrochlore phase. The dielectric, piezoelectric, ferroelectric and pyroelectric properties of (100–x)PMN–xPT ceramics were systematically studied.

2. Experimental Procedure

The (100–x)$PbMg_{1/3}Nb_{2/3}O_3$–$xPbTiO_3$ (designated as PMN–xPT, with x = 24, 25, and 26) ceramics were prepared using the traditional solid-state reaction method. The Pb_3O_4 (99.95%), $C_4H_6MgO_4{\cdot}4H_2O$ (99%), Nb_2O_5 (99.9%), TiO_2 (99%) were used as raw materials. All the raw materials are purchased from Aladdin reagent. First, $C_4H_6MgO_4{\cdot}4H_2O$ and Nb_2O_5 were weighed according to the chemical reaction of Eq. (1). The powder mixtures were ball-milled for 24 h, then dried and heated to 1000°C at a rate of 5°C/min, and held for 6 h. The $MgNb_2O_6$ precursor was obtained. Second, according to the stoichiometric ratio, the synthesized $MgNb_2O_6$ was mixed with Pb_3O_4 and TiO_2, and ball-milled for using alcohol as solvent for 24 h. 10 mol.% Pb_3O_4 and 5 mol.% $C_4H_6MgO_4{\cdot}4H_2O$ was additionally added to compensate for the possible volatilization of Pb and Mg element during heat treatment. The mixed power was dried, and then calcined at 800°C for 2 h, Afterwards, the calcined powder went through a second ball milling for 24 h. Then, the resultant powder was mixed with 7% concentration of polyvinyl alcohol (PVA). The powder was pressed into green pellets with a diameter of 10 mm and a thickness of 1.5 mm by isostatic pressing. Finally, these samples were sintered at 1220°C for 2 h.

$$C_4H_6MgO_4{\cdot}4H_2O + Nb_2O_5 + 4O_2 \rightarrow MgNb_2O_6 + 7H_2O + 4CO_2. \quad (1)$$

The crystal structure of the PMN–xPT was analyzed by X-ray diffractometer (XRD; D8 ADVANCE, Bruker, Germany) using Cu Kα radiation (λ = 0.15418 nm) at a scanning speed of 0.2°/s, a step size of 0.02° and a scanning range of 20°– 80°. The morphology and grain size of the ceramics were characterized by field emission scanning electron microscope (FESEM; SU8220, Hitachi, Japan). The density of the sample was measured by water immersion technique using Archimedes' principle. The instrument used to collect the dielectric property data was Agilent E4981A capacitance meter, which was tested at 1 kHz. The instrument used to obtain the dielectric temperature spectrum data was TH 2816 A digital bridge. The piezoelectric constant d_{33} of the sample was measured with a quasi-static d_{33} measuring instrument (JZ-3AN, Institute of Acoustics Academic, China). The polarization hysteresis loops (P–E), strain-electric field (S–E), d_{33}-electric field (d_{33}–E) and ε_r-electric field (ε_r–E) curves of the ceramics were measured using a ferroelectric analyzer TF-1000 (Aixacct, Germany).

3. Result and Discussion

Figure 1 shows the XRD patterns of as-received PMN–xPT ceramics with different PT contents. The diffraction profiles reveal that PMN-25PT has a single perovskite structure, but

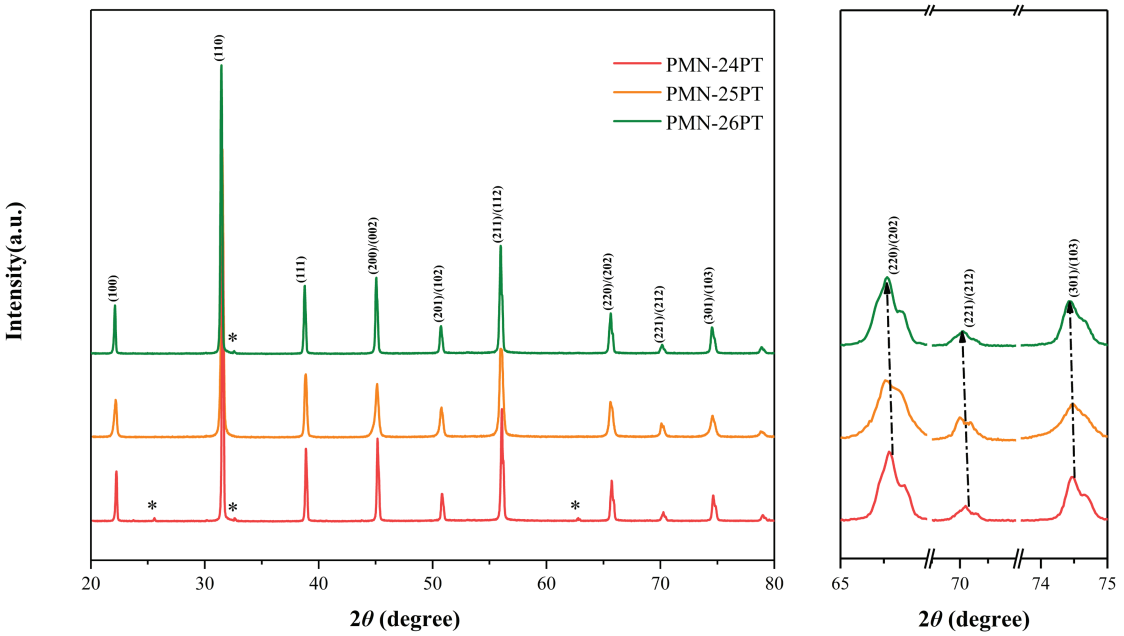

Fig. 1. XRD patterns of PMN–xPT ceramics sintered at 1220°C for 2 h: (a) 20°–80° and (b) 65°–75°.

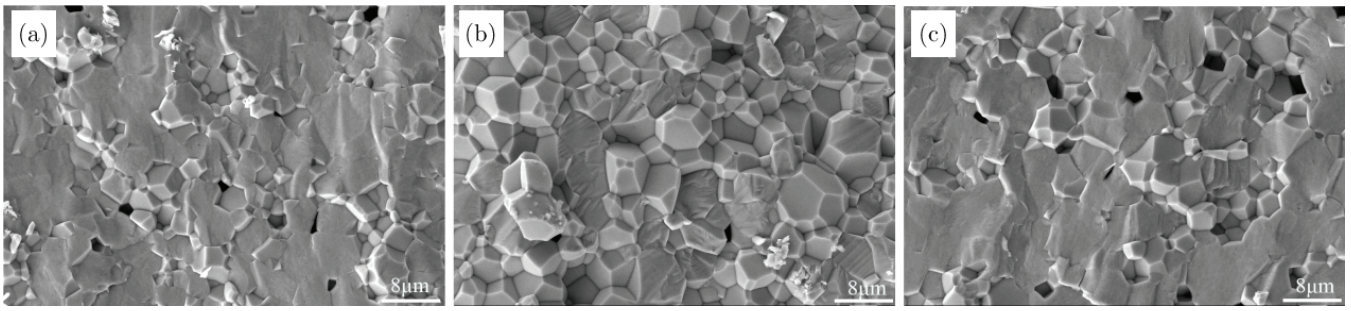

Fig. 2. SEM micrographs of PMN–xPT ceramics sintered at 1220°C for 2 h: (a) PMN–24PT, (b) PMN–25PT and (c) PMN–26PT.

a trace amount of pyrochlore phase (marked as *) is present in PMN-24PT and PMN-26PT. It suggests that for the case of PMN-25PT, the PT can form a complete solid solution with the PMN matrix. In order to analyze the process of structural change further in detail, three characteristic reflection peaks, {220}, {221} and {301} in the range from 65° to 75° are chosen, as shown in Fig. 1(b). With increasing PT concentration, they are split into {220}, {221} and {301} peaks for all the ceramics, which suggests that rhombohedral and tetragonal phases coexist in all these components. In addition, {202}, {212} and {103} peaks shift towards lower angle, implying the expansion of lattice due to the incorporation of PT. Therefore, the addition of PT changes the phase structure, which would have an impact on the piezoelectric, dielectric and pyroelectric properties of materials.

In order to analyze the morphology of the PMN–xPT ceramics, field emission scanning electron microscopy (FESEM) was used. Figure 2 presents the microstructure of PMN–xPT ceramics. All of the samples have dense microstructure with well-defined grains and very small amount of pores with a high relative density (>95%). However, compared with other samples, PMN-25PT has good grain development, full crystal shape and clear grain boundary contour (the average grain size of 5.53 μm), indicating that PMN-25PT ceramic has the highest crystallization degree. With the increase of PT content, it is found that the average grain size increases, the grain distribution gets uniform and the grain gradually becomes round. According to the existing research results,[22–25] the grain size will affect the piezoelectric and dielectric properties of ceramics. Under a certain grain size, it increases with the increase of grain size. If it exceeds this critical value, it will decrease with the increase of grain size.

Figures 3(a)–3(c) show the temperature-dependent dielectric permittivity and loss tangent of PMN–xPT ceramics measured from 30°C to 140°C at 1 kHz, 10 kHz and 100 kHz, respectively. All the samples display obvious frequency dispersion, suggesting the nature of the relaxor state. However, two anomalies are observed in the dielectric permittivity curves. The one at the lower temperature region (~80°C) could be attributed to the process of thermal evolution of

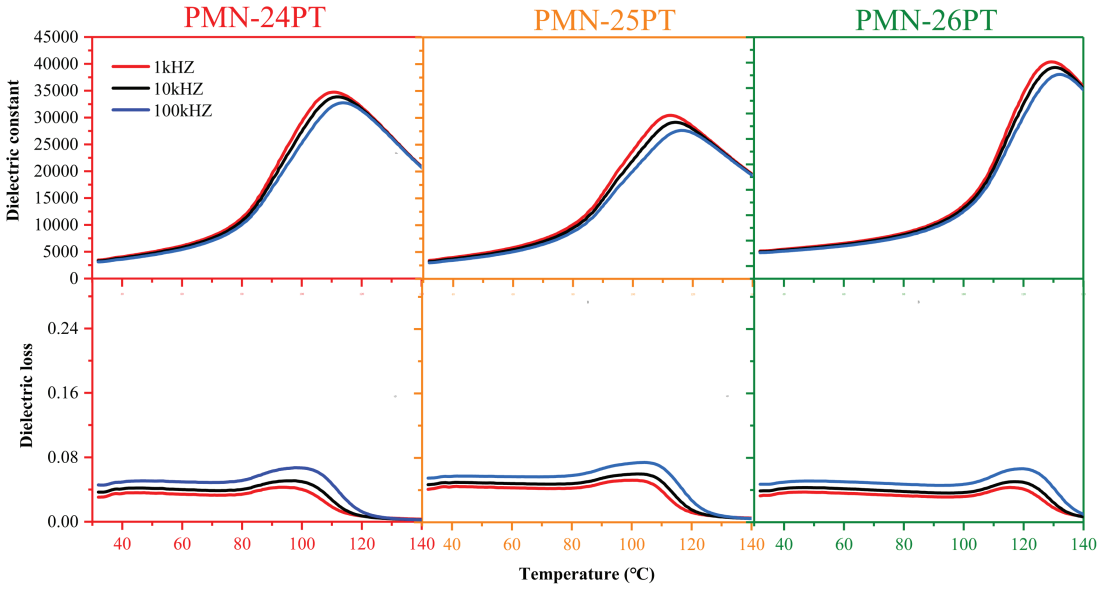

Fig. 3. Temperature dependence of dielectric permittivity and tangent loss at different measuring frequencies for (a) PMN–24PT, (b) PMN–25PT and (c) PMN–26PT.

discrete tetragonal polar nanoregions (PNRs).[26] The other one at the higher temperature region (~110°C) can be designated as T_m with the maximum value of the dielectric permittivity, corresponding to the PNRs relaxation emerged from rhombohedral PNRs.[27,28] As the frequency decreases, T_m moves to lower temperature, indicating that all samples are relaxor ferroelectrics. Moreover, with the increase of PT content, ε_r of the sample first decreases and then increases, and tanδ also shows the same trend. The overall dielectric frequency dispersion decreases and T_m increases linearly.

Figure 4(a) displays the polarization hysteresis loops (P-E) for PMN–xPT measured under 2 kV/mm. It is observed that the remnant polarization P_r of the ceramics decreases with the increase of PT content. On the one hand, this can be attributed to the change of crystal structure. Through the above analysis of permittivity results, it can be seen that with the increase of PT content, the relaxation characteristics increase, which will seriously damage the long-range order of the original oxygen octahedron, thereby reducing the stability of the ferroelectric unit and damaging the inherent ferroelectricity.[29] On the other hand, the introduction of PT destroys long-range ordered ferroelectric domains and weakens the stability of coupling between charged defective dipoles and domains. Figure 4(b) presents the electric field-induced strains at room temperature for PMN–xPT ceramics. With the increase of PT content, the strain increases, while the overall strain remains a relatively high value (>0.08%, at 2 kV/mm). Symmetric butterfly-shaped loop, a characteristic of good piezoelectric system, is observed, which establishes the utility of PMN–xPT ceramics for actuator applications. The effective piezoelectric coefficient d_{33} of PMN–xPT ceramics as a function of electric field d_{33}-E curves is shown in Fig. 4(c). It can be seen that the d_{33}-E curve of the sample follows the standard ferroelectric hysteresis loop shape. The maximum piezoelectric

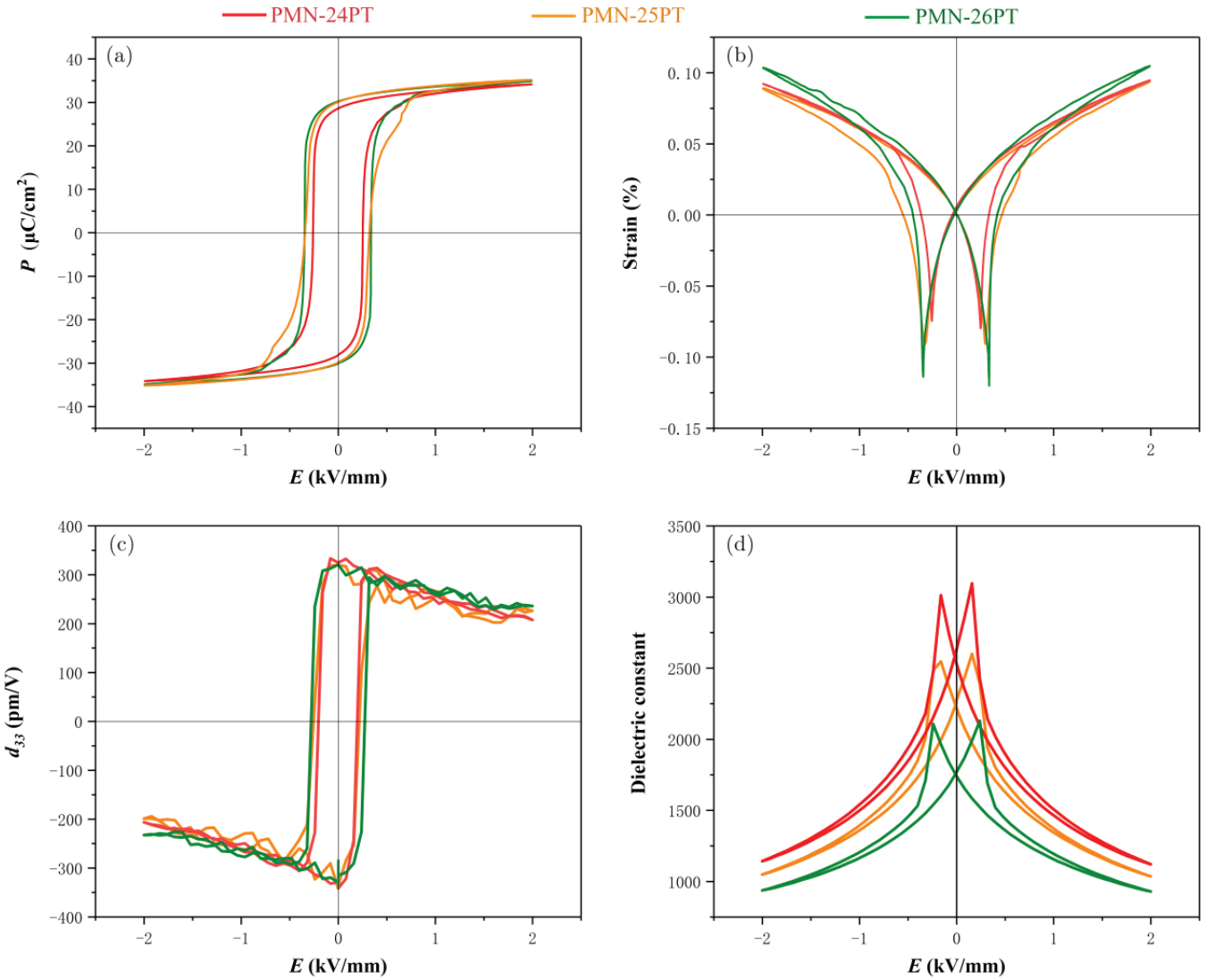

Fig. 4. The (a) P–E loops, (b) S–E loops, (c) d_{33}–E loops and (d) ε_r–E loops of PMN–xPT ceramics.

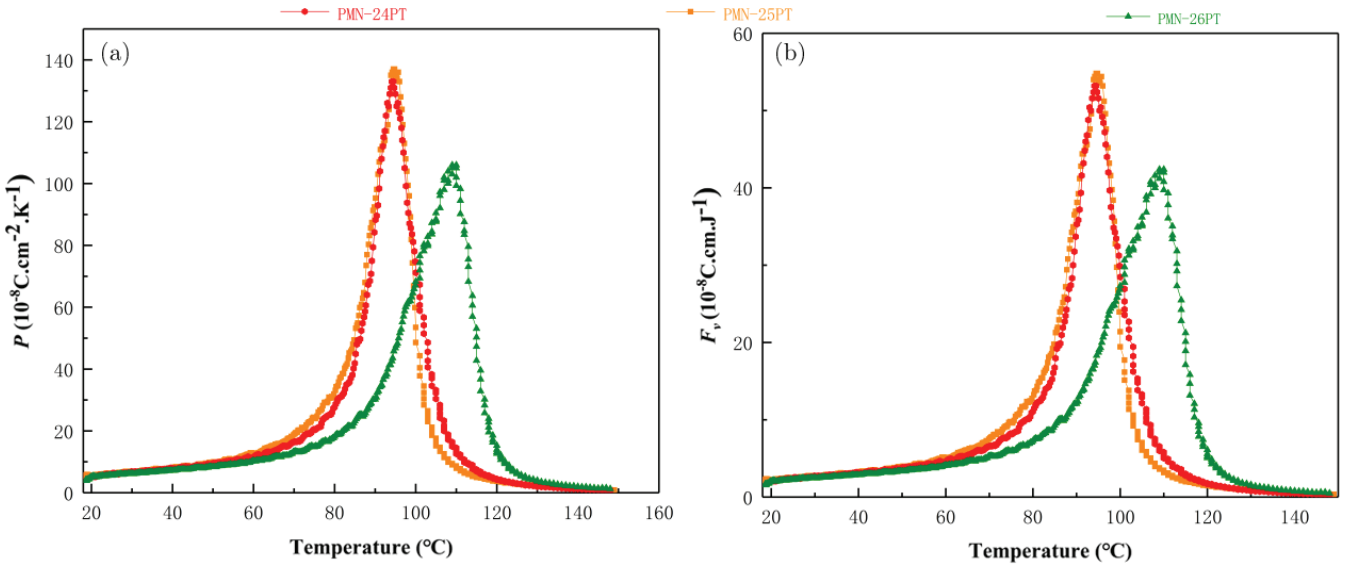

Fig. 5. Pyroelectric constant and F_v as a function of temperature for PMN–xPT ceramics.

coefficient reaches 320 pm/V, and with the increase of PT content, its value increases, due to the increase of relaxation, being consistent with the previous *P-E* diagram. It can be seen from Fig. 4(d) that the dielectric constant decreases with the PT content at zero bias voltage, and the dielectric response is the largest when the PT content is 25. With the increase of bias field, the difference of dielectric response decreases gradually, which is analogous to the changing trend of the C–V characteristics of the PZT system with composition in the literatures[30,31] (the dielectric response is the largest at zero bias field, and the difference decreases gradually with the increase of bias field). According to the maximum dielectric response at the low bias field of PMN–25PT, this component has the largest contribution of domain wall motion. However, the domain wall motion will be frozen by the bias field. When the bias field increases, the contribution of the domain wall motion to the dielectric response decreases gradually. The dielectric response also decreases with the change of composition.

The pyroelectric coefficient and voltage response F_v of PMN–xPT ceramics are investigated, as shown in Figs. 5(a) and 5(b), respectively. It can be seen from Fig. 5(a) that the pyroelectric coefficient decreases slightly with the increase of PT content at room temperature. However, the pyroelectric coefficient of the ceramic system remains in the range of 5.5–6.3 × 10^{-8} C·cm^{-2}·K^{-1}, indicating that the pyroelectric coefficient of the ceramic system can be maintained in a stable range. At the same time, the peak p_{max} of the pyroelectric coefficient also shows similar changes at the $F_{RL} - F_{RH}$ phase transition temperature. However, it can be seen that the position of p_{max} peak of PMN–26PT ceramics is obviously different from that of other components. Because the composition of PMN–26PT ceramic was very close to the MPB region, so it has a high $F_{RL} - F_{RH}$ phase transition temperature, which is also consistent with the results of the dielectric spectrum. The curve in Fig. 5(b) shows the variation of the optimal voltage response value F_v of the sample with temperature, which is consistent with the variation of pyroelectric coefficient. At room temperature, the voltage response F_v of the ceramic system is between 2.1–2.5 × 10^{-8} C·cm·J^{-1}.

4. Conclusion

The phase structure, microstructure and electrical properties of PMN–xPT ceramics were systematically investigated in this study. Well-shaped and saturated *P–E* hysteresis loops with high room temperature remnant polarization, a high electro-strain of 0.08% at 2 kV/mm, and effective piezoelectric coefficient of 320 pm/V could be obtained. The PMN–xPT ceramics are found to have a very high pyroelectric coefficient of 5.5–6.3 × 10^{-8} C·cm^{-2}·K^{-1} and F_v of 2.1–2.5 × 10^{-8} C·cm·J^{-1} at room temperature. The results suggest that PMN–xPT ceramics are promising candidates for piezoelectric and pyroelectric applications.

Acknowledgment

This work was supported by the State Grid Corporation of China through the Project No. 5500-202058320A-0-0-00.

References

[1]B. Jaffe, H. Jaffe, W. R. Cook, *Piezoelectric Ceramics* (Academic Press, London, 1971).
[2]S. W. Choi, T. R. Shrout, S. J. Jang and A. S. Bhalla, Morphotropic phase boundary in Pb($Mg_{1/3}Nb_{2/3}$)O_3-$PbTiO_3$ system, *Mater. Lett.* **8**, 253 (1989).
[3]D. Lin, Z. R. Li, F. Li, Z. Xu and X. Yao, Characterization and piezoelectric thermal stability of PIN-PMN-PT ternary ceramics

near the morphotropic phase boundary, *J. Alloy. Compd*. **489**, 115 (2010).
[4]A. S. Bhalla, R. Guo and E. F. Alberta, Some comments on the morphotropic phase boundary and property diagrams in ferroelectric relaxor systems, *Mater. Lett*. **54**, 264 (2002).
[5]A. Sanchez, C. Zambrano, L. M. Procel and A. Stashans, Structural and Electronic Properties of PZT, *Conference on Advanced Organic and Inorganic Optical Materials*. 310 (2002).
[6]V. A. Isupov, Reasons for discrepancies relating to the range of coexistence of phases in lead zirconate–titanate solid solutions, *Sov. Phys. Solid State*. **22**, 98 (1980).
[7]V. A. Isupov, Phases in the PZT ceramics, *Ferroelectrics* **266**, 91 (2002).
[8]Q. H. Guo, L. T. Hou, F. Li, F. Q. Xia, P. B. Wang, H. Hao, H. J. Sun, H. X. Liu and S. J. Zhang, Investigation of dielectric and piezoelectric properties in aliovalent Eu^{3+}-modified $Pb(Mg_{1/3}Nb_{2/3})O_3$-$PbTiO_3$ ceramics, *J. Am. Ceram. Soc*. **102**, 7428 (2019).
[9]H. Fu and R. E. Cohen, Polarization rotation mechanism for ultrahigh electromechanical response in single-crystal piezoelectrics, *Nature* **403**, 281 (2000).
[10]M. Promsawat, A. Watcharapasorn, Z.-G. Ye and S. Jiansirisomboon, Enhanced dielectric and ferroelectric properties of $Pb(Mg_{1/3}Nb_{2/3})_{0.65}Ti_{0.35}O_3$ ceramics by ZnO modification, *J. Am. Ceram. Soc*. **98**, 848 (2015).
[11]C. He, Z. J. Wang, X. Z. Li, Y. Liu, D. Q. Shen, T. Li and X. F. Long, Synthesis, structure and electric properties of $Pb(Yb_{1/2}Nb_{1/2})O_3$-$Pb(Mg_{1/3}Nb_{2/3})O_3$-$PbTiO_3$ ternary ceramics, *J. Phys. D. Appl. Phys*. **45**, 105305–1 (2012).
[12]S. W. Choi, RT. R. Shrout, S. J. Jang and A. S. Bhalla, Dielectric and pyroelectric properties in the $Pb(Mg_{1/3}Nb_{2/3})O_3$-$PbTiO_3$ system, *Ferroelectrics* **100**, 29 (1989).
[13]A. Benayad, D. Kobor, L. Lebrun, B. Guiffard and D. Guyomar, Characteristics of $Pb[(Zn_{1/3}Nb_{2/3})_{0.955}Ti_{0.045}]O_3$ single crystals versus growth method, *J. Cryst. Growth* **270**, 137 (2004).
[14]J.A. Lima, W. Paraguassu, P. T. C. Freire, A. G. Souza Filho and J. A. Eiras, Lattice dynamics and low-temperature Raman spectroscopy studies of PMN-PT relaxors, *J. Raman Spectrosc*. **40**, 1144 (2009).
[15]Z. Li, L. Zhang and X. Yao, Dielectric properties anomaly of $(1-x)$-$Pb(Ni_{1/3}Nb_{2/3})O_3$-$x PbTiO_3$ ceramics near the morphotropic phase boundary, *J. Mater. Res*. **16**, 834 (2001).
[16]Z. Z. Xi, Q. Q. Bu, P. Y. Fang, W. Long and X. J. Li, Effect of frequency and temperature on dielectric relaxation of [111]-oriented PMN-32PT single crystals, *J. Alloy. Compd*. **618**, 14 (2015).
[17]R. Guo, C.-A. Wang and A. K. Yang, Effects of pore size and orientation on dielectric and piezoelectric properties of 1–3 type porous PZT ceramics, *J. Eur. Ceram. Soc*. **31**, 605 (2011).
[18]Y. L. Qin, F. X. Han, P. K. Yan, Y. Q. Wang, Y. C. Zhang and S. J. Zhang, Fluorescence intensity ratio (FIR) analysis of the temperature sensing properties in transparent ferroelectric PMN-PT: Pr^{3+} ceramic, *Ceram. Int*. **47**, 24092 (2021).
[19]P. Kumar, S. Sharma, O. P. Thakur, C. Prakash and T. C. Goel, Dielectric, piezoelectric and pyroelectric properties of PMN–PT (68:32) system, *Ceram. Int*. **30**, 585 (2004).
[20]P. Augustine and M. S. R. Rao, Realization of device quality PMN–PT ceramics using modulated heating method, *Ceram. Int*. **41**, 11984 (2015).
[21]Z. Q. Zhang, F. Li, R. M. Chen, T. F Zhang, X. D. Cao, S. J. Zhang, T. R. Shrout, H. R. Zheng, K. K. Shung, M. S. Humayun, W. B. Qiu, Q. F. Zhou, High-performance ultrasound needle transducer based on modified pmn-pt ceramic with ultrahigh clamped dielectric permittivity, *IEEE Trans. Ultrason. Ferroelectr. Freq. Control*. **65**, 223 (2018).
[22]A. Hussain, Abid Hussaina, N. Sinha, S. Bhandari, H. Yadav and B. Kumar, Synthesis of $0.64Pb(Mg_{1/3}Nb_{2/3})O_3$-$0.36PbTiO_3$ ceramic near morphotropic phase boundary for high performance piezoelectric, ferroelectric and pyroelectric applications, *J. Asi. Ceram. Soc*. **4**, 337 (2016).
[23]F. F. Wang, H. N. Wang, Q. S. Yang, Z. X. Zhang and K. Yan, Fine-grained relaxor ferroelectric PMN-PT ceramics prepared using hot-press sintering method, *Ceram. Int*. **47**, 15005 (2021).
[24]V. Kalem, W. Y. Shih and W. H. Shih, Dielectric and piezoelectric properties of PMN-PT ceramics doped with strontium, *Ceram. Int*. **44**, 2835 (2018).
[25]M. Unruan, S. Unruan, Y. Inkong and R. Yimnirun, Estimation of energy density of PMN-PT ceramics utilizing mechanical stress, *Integr. Ferroelectr*. **195**, 39 (2019).
[26]V. V. Shvartsman and D. C. Lupascu, Lead-free relaxor ferroelectrics, *J. Am. Ceram. Soc*. **95**, 1 (2012).
[27]A. A. Bokov, H. Luo and Z. G. Ye, Polar nanodomains and relaxor behaviour in $(1-x)Pb(Mg_{1/3}Nb_{2/3})O_3$-$xPbTiO_3$ crystals with x = 0.3–0.5, *Mater. Sci. Eng. B*. **120**, 206 (2005).
[28]A. A. Bokov and Z. G. Ye, Recent progress in relaxor ferroelectrics with perovskite structure, *J. Mater. Sci*. **41**, 31 (2006).
[29]L Jin, F. Li and S. J. Zhang, Decoding the fingerprint of ferroelectric loops: Comprehension of the material properties and structures, *J. Am. Ceram. Soc*. **97**, 1 (2014).
[30]W. H. He, Q. Li, Q. F. Yan, N. N. Luo, Y. L. Zhang, X. C. Chu and D. H. Shen, Temperature-dependent phase transition in orthorhombic $[011]_c$ $Pb(Mg_{1/3}Nb_{2/3})O_3$-$0.35PbTiO_3$ single crystal, *Crystals* **4**, 262 (2014).
[31]G. Du, R. H. Liang, L. Wang, K. Li, W. B. Zhang, G. S. Wang and X. L. Dong, Linear temperature scaling of ferroelectric hysteresis in Mn-doped $Pb(Mn_{1/3}Sb_{2/3})O_3$-$Pb(Zr,Ti)O_3$ ceramic with internal bias field, *Appl. Phys. Lett*. **102**, 142903 (2013).